ISSN: 1674-8190

Design of Current-Mode Instrumentation Amplifiers for ECG Signal Acquisition Using 0.25µM CMOS Technology

Lucas Martinez¹, Daniel Martinez¹, Olivia Adams²

- ¹ Department of Sociology, University of California, Los Angeles, USA
- ² School of Environmental Science, University of Melbourne, Australia

KEYWORDS: Instrumentation Amplifiers, Current-Mode, Rail-to-Rail Op-Amps, Current Conveyors, ECG.

ABSTRACT

Four monolithic current-mode instrumentation amplifier (in-amp) topologies implemented in a standard $0.25\mu m$ complementary metal-oxide semiconductor (CMOS) process, with positive second-generation current conveyors (CCII+) as building blocks are presented in this paper. The in-amp topologies are designed to handle biomedical signals, specifically that of the electrocardiogram (ECG). Four types of CCII+ are characterized and realized using a rail-to-rail operational amplifier (op-amp) and different types of current mirrors. The Op-Amp with Simple Current Mirror exhibits the highest current swing and the lowest power consumption, and is thus chosen as the optimum CCII+ block to be used in all four in-amps. All current-mode in-amps yield excellent common-mode rejection ratio (CMRR) greater than 150dB for a differential gain of 100. The in-amps consume less than 2.5mW of power for a single voltage supply of 2.5V. However, the 2-Current Conveyor with Op-Amp at the Output (2-CC with Op-Amp) has adjustable output reference voltage and provides the lowest output impedance among the four in-amps.

INTRODUCTION

The measurement of low-energy bio-potential signals such as the electrocardiogram (ECG) makes the instrumentation amplifier (hereinafter referred to as in-amp) a significant signal-conditioning block for biomedical systems. With the use of in-amps, it is possible to accurately amplify these weak electric body signals even in the presence of high-amplitude common-mode noise that may tend to corrupt the desired signal. Having this critical application, in-amps are particularly designed to achieve high common-mode rejection ratio (CMRR) to correctly extract and amplify low-amplitude differential signals, and to block unwanted noise potentials that are usually common to the in-amp inputs [1], [2].

Recent works have explored alternative ways to implement in-amps using the current-mode approach to overcome the requirement for matched resistors [3]. One approach is through the use of current conveyors.

Vital parameters for characterization and analysis of in-amps include CMRR, input and output impedance, input and output swing, and power consumption. A simulated ECG signal with common-mode noise is used in simulating these different in-amp circuits to determine which in-amp configuration could best extract these biomedical signals.

CURRENT CONVEYORS

A positive second-generation current conveyor (CCII+) is a 3-terminal device with a representation in Fig. 1.

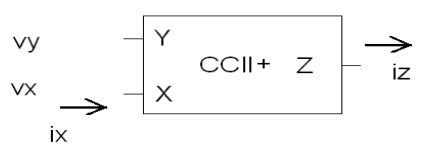


Fig. 1. CCII+ block diagram.

Current conveyor performance relies on its ability to act as a voltage buffer between inputs, and to convey current between two ports that have extremely different impedance levels. To realize this, a complementary metal-oxide semiconductor (CMOS) second-generation current conveyor (hereinafter referred to as CCII+) can be implemented by a high gain operational amplifier (hereinafter referred to as op-amp) with a class AB output buffer stage, and connected with a negative-feedback loop, followed by a current mirror [4], as shown in Fig. 2.

ISSN: 1674-8190

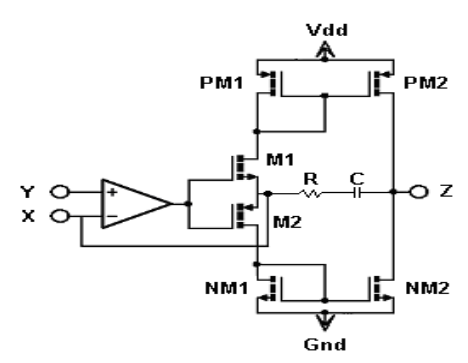


Fig. 2. CCII+ block with series-RC compensation.

Op-amp block

To implement a CCII+, the *Complementary Differential Pair with NMOS Cascode Load (ComdiffCasc-PN) with Push-Pull Inverter Output Stage* [5] shown in Fig. 3, is the topology used as the op-amp block.

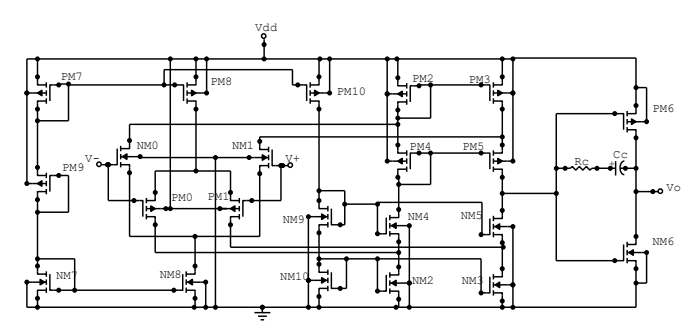


Fig. 3. ComdiffCasc-PN with push-pull inverter output stage.

The op-amp has rail-to-rail swing at both the input and output and has fewer stages than the other rail-to-rail op-amp configurations in [4], which makes it more stable. Also, its push-pull output stage further improves the differential gain and provides higher output voltage swing.

Setting all the transistor lengths (L) to $1.2\mu m$, the initial op-amp transistor widths (W) may be solved using the current equation, given in Eq. 1, for a MOSFET in saturation. The reason for choosing the $1.2\mu m$ transistor length, instead of the minimum length of $0.25\mu m$, is that short-channel effects are more significant at channel lengths less than 1um. Furthermore, submicron lengths for differential input pairs tend to introduce large offset voltage [6]. The tail current (I_{bias}) is set to be $20\mu m$ to minimize the total current and to meet the power consumption limits.

$$I_{D} = \frac{k'W}{2L} (V_{GS} - V_{T})^{2}$$
 (1)

A width of $5\mu\text{m}/20\mu\text{m}$ is used for NMOS/PMOS transistors with $I_{\text{bias}}/2$ current. Plugging these values into the schematic produced an op-amp differential voltage gain of less than 10,000, which is below the target gain of at least $1x10^6$. The transistor widths are then resized to increase the gain. A series of simulations aimed at characterizing the op-amp were carried out. The effects of varying the width of each transistor on the op-amp parameters such as differential gain, common-mode gain, 3-dB bandwidth, unity-gain bandwidth and phase margin were studied and plotted. Finally, transistor sizes were assumed to be multiples of 6, to aid in the layout implementation. The compensation resistor (R_C) and capacitor (R_C) used were R_C 0 and R_C 10 used were R_C 20 used were R_C 30 used were R_C 40 used R_C 40 used were R_C 40 used R_C 40 used R_C 40 used R_C 40 used R_C 40

Due to parasitics introduced by metal layers, the total output resistance in the layout simulations increased, as compared to schematic simulations – thus increasing the differential gain. However, slight mismatches in the layout and the lack of symmetry in routing also increased the common-mode gain, hence decreasing the CMRR.

Furthermore, these parasitics introduce more poles, thus decreasing the bandwidth of the op-amp. It was also observed that the phase margin of the layout implementation is 20° lower than that of schematic simulations. As such, it is suggested that the phase margin be set at a relatively high value early in the schematic design stage to ensure stability in the layout stage.

Current conveyor block

ISSN: 1674-8190

The designed rail-to-rail op-amp is then connected to an output buffer stage before being paired with four types of current mirrors, which are: *Simple Current Mirror*, *Cascode Current Mirror*, *High-Swing Cascode Current Mirror* and *Wilson Current Mirror*. The requirements for the current mirrors to be used for the CCII+ are high output impedance, wide output voltage swing, small input bias voltage, and good high frequency response [7].

Even though the *Op-Amp with Simple Current Mirror* displayed the lowest output impedance among the four CCII+ implementations, it provided the highest current swing and had the least layout area and power consumption (having the least number of transistors) among all designs.

The positive input signal swing is determined by the state of transistor M1 while the negative input signal swing is determined by M2, as shown in Fig. 2. To have a functional output buffer stage, transistors M1 and M2 in Fig. 2 must remain saturated [7]. Therefore, the positive and negative input signal swing is restricted by Eq. 2-3.

$$V_{IN}^{+} = V_{DD} - V_T - V_{DSAT} - V_{DSAT1}$$
 (2)

$$V_{IN}^{-} = V_{DSAT2} + V_T + V_{DSAT} \tag{3}$$

To minimize the voltage drop across the mirrors, the width of the transistors comprising the current mirrors is increased. This decreases the required V_{GS} for saturation. Hence, decreasing the input bias voltage requirements of the current mirrors increases the input swing at node X in Fig. 2. For uniformity and ease of layout, the widths of all the NMOS and PMOS transistors for the simple current mirrors are set to be $48\mu m$ and $192\mu m$ respectively.

CURRENT-MODE INSTRUMENTATION AMPLIFIERS

Initial simulations on the *Improved 2-Current Conveyor (Improved 2-CC)* in-amp, shown in Fig. 4, verified the functionality of the *Op-Amp with Simple Current Mirror*. The in-amp produced a very high CMRR. However, it was observed from the in-amp's gain plot that the differential gain varies with the differential input voltage by $\pm 10\%$. This gain irregularity is explained by the current error of the CCII+ (difference in current at the Z and X terminals). Ideally, the current at the output node Z of the conveyor follows the current at the input X but based on simulations, the current error increases as differential input is increased.

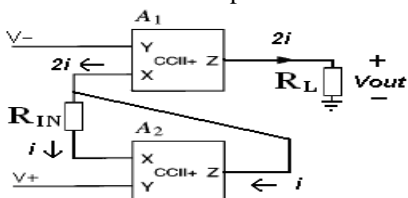


Fig. 4. Improved 2-CC schematic design [8].

Stability was compromised due to the multiple stages employed in the CCII+ implementation. A series-RC compensation was placed between the buffer stage output and the current conveyor output node Z for all the CCII+ blocks used in all the in-amp circuits. The compensating resistor was set to $1K\Omega$ while the compensating capacitor was limited to 2pF due to lay-out area considerations.

The 2-Current Conveyor (2-CC) is the most basic current-mode implementation of the in-amp. Any voltage difference applied between the in-amp inputs V+ and V- will also be reflected across R_{IN} , forcing a current through it.

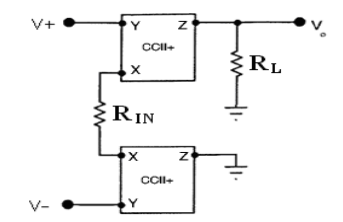


Fig. 5. 2-CC schematic design [3].

By the operation of the CCII+, this same current will be conveyed and will then flow through R_L . It can be derived that the differential voltage gain of this topology is

$$A_{VD} = \frac{V_{OUT}}{(V_{-}) - (V_{+})} = \frac{R_L}{R_{IN}}$$
 (4)

ISSN: 1674-8190

The resistors chosen for this circuit were $50K\Omega$ for R_L (as in the other topologies) and 500Ω for R_{IN} to achieve a gain of 100. A large value of R_L was needed to make the output voltage swing approach the supply rail despite the low current being passed at the output.

The configuration in Fig. 6 is an improvement to the 2-CC in-amp. As seen, an op-amp is added as an output stage to decrease the output impedance of the in-amp circuit. This op-amp, A_3 , is chosen to be tied at the output of the conveyor A_2 to produce a positive gain. As in the previous topology, the differential gain is given in Eq. 4.

The cascaded op-amp A_3 is the same op-amp used in the CCII+ implementation, with the same sizing and biasing. However, it was necessary to increase the compensation of the op-amp to make the 2-Current Conveyor with Op-Amp at the Output (2-CC with Op-Amp) stable. The op-amp's C_C was increased from 500fF to 2pF, while R_C was increased from $10K\Omega$ to $20K\Omega$.

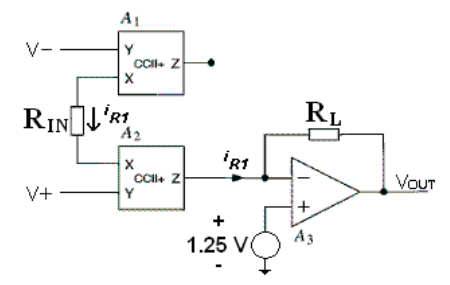


Fig. 6. 2-CC with op-amp at the output schematic design [4].

The positive terminal of A_3 must be biased to at least V_{DSAT} , instead of just being grounded. This is to ensure that the output current mirrors of the conveyor A_2 have enough drain-source bias to maintain saturation, and thus enables the conveyor A_2 to properly mirror current i_{R1} . In this design, a 1.25V-bias serves two purposes – aside from ensuring that conveyor A_2 effectively mirrors the current i_{R1} , it also raises the in-amp's output reference voltage to 1.25V, placing the output reference exactly between the rails. The 1.25V could be derived from the 2.5 V_{DD} through voltage dividers.

The *Improved 2-CC*, shown in Fig. 4, is typified by a feedback loop from the unloaded output of A_2 to the X terminal of A_1 . Effectively, the voltages V- and V+ are imposed on the opposite ends of R_{IN} and determines the value of the current *i*. This same current is forced to flow into the Z terminal of A_2 . Therefore, the total current leaving the X and Z terminals of A_1 is 2i. A_{VD} can be calculated to be,

$$A_{VD} = \frac{Vout}{(V_{-}) - (V_{+})} = 2\frac{RL}{R_{IN}}$$
 (5)

The 3-Current Conveyor (3-CC) topology consists of three CCII+'s and two resistors, with current conveyors B and C cascaded. As seen in Fig. 7, the current entering R_L is twice the current entering R_{IN} , so A_{VD} can be shown in Eq. 5.

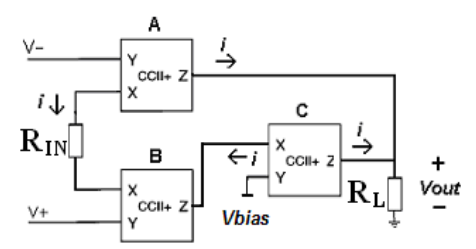


Fig. 7. 3-CC schematic design [9].

The CCII+ labeled as C, has V_{BIAS} at its Y terminal instead of being directly grounded. Again, this is to ensure that there is enough V_{DS} at the output current mirrors of conveyor B. As done previously, V_{BIAS} was set to 1.25V.

REPRESENTATION OF THE ECG SIGNAL

A representation of an ECG waveform using a piece-wise linear voltage source file is employed to verify the capability of the in-amps to accurately amplify ECG signals amidst common-mode noise. The model used in

ISSN: 1674-8190

plotting the signal is adapted from related literature on biomedical signals. In addition, the simulated ECG signal was made to last for only 3 periods, so that simulations would not take much time.

Common-mode noise was added to the ECG signal, as a cascade of 100mV-sinusoids at 60, 120, 180 and 240Hz. A 1.25V DC voltage source was also used as a commode-mode input voltage to maintain correct biasing of the in-amp.

RESULTS AND ANALYSIS

All the current-mode in-amp topologies achieved the fixed differential gain of 100, a superior CMRR of at least 150dB, and very high input impedance in the $G\Omega$ -range. However, the in-amps failed to provide a rail-to-rail input voltage signal swing because of the input signal constraints of the current conveyors. Hence, to allow the μV -range signal level of the ECG as input to the in-amps, the 1.25V DC input common-mode voltage was necessary.

No significant difference is observed between the 2-CC and the *Improved* 2-CC in-amps. Both topologies consume less power because they have fewer components compared to the other two topologies. The only difference between them is that the 2-CC has a greater tendency to suffer crosstalk due to the unused output of one of its conveyor blocks. The 3-CC in-amp, on the other hand, also produces the same performance despite the additional conveyor. Simulations have shown that aside from failing to produce an evident improvement in results, the third conveyor also degrades the bandwidth of the circuit and consumes more power.

The 2-CC with Op-Amp in-amp provides the smallest output impedance because of the addition of an op-amp as an output stage. Furthermore, this topology has an easily adjustable output reference voltage.

Shown in Table 1 is the comparison between the achieved parameters of the 2-CC with Op-Amp and the specifications of the INA326 [10], which is also a current-mode in-amp.

Table 1 Parameters of 2-CC with Op-Amp vs. INA326.

Tuble 11 drameters of 2-cc with Op-11th vs. 1141320.		
Parameters	2-CC with Op-Amp	INA326
Differential gain	102.92	0.1 to 10000
Common-mode gain	4.16E-7	1.995E-04
CMRR	167.87dB	114 dB
Output voltage swing Range	6.14mV to 2.46V	Vss+10mV to Vdd-10mV
Input offset voltage	-3.24 uV	100uV
Supply current	798.51uA	2.4mA
Power consumption	1.99mW	Current*(± 2.7 to ± 5.5)
$R_{\rm IN}^+,R_{\rm IN}^-$	$794G\Omega$, $792G\Omega$	$100G\Omega$, $100G\Omega$
R_{OUT}	58.49Ω	
3-dB bandwidth	1.26MHz	1KHz
PSRR @ 60Hz	85.68dB	110dB
Settling time	639.28ns	0.95ms
Slew rate	1.9V/us	Filter limited

Meanwhile, shown in Fig. 8 is the output plot obtained as the 2-CC with Op-Amp is applied with the simulated ECG signal and common-mode noise. Clearly, it can be seen that the in-amp has indeed rejected the common-mode signals incorporated in the simulated ECG signal.

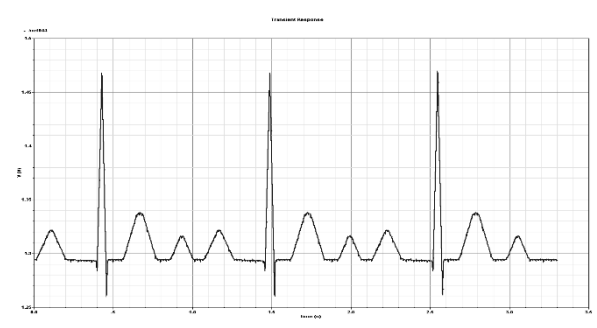


Fig. 8. Output of 2-CC with Op-Amp with input ECG signal and noise.

ISSN: 1674-8190

CONCLUSION

In-amp designs should always take into account the trade-off between CMRR and stability. Simulations showed that a decrease in the common-mode gain increases the CMRR, thus compromising stability. Generally, cascading more stages to improve certain parameters, such as CMRR, worsens the stability of a system.

All the current-mode in-amp topologies achieve impressively high CMRR. Hence, any of the implemented current-mode circuits is an outstanding differential amplifier and thus, a potential ECG system block. However, the 2-CC with Op-Amp provides the lowest output impedance that is essential for connecting the in-amp into a larger system. It also has the advantage of being able to adjust its output reference voltage, allowing it to handle both negative and positive signals with respect to the reference voltage.

ACKNOWLEDGMENTS

The authors would like to express gratitude to Microelectronics and Microprocessors Laboratory of the University of the Philippines for the technical support during the course of the design and study. Author F. Gomez would like to extend appreciation to the STMicroelectronics Calamba NPI Team and the Management Team for the utmost support.

REFERENCES

- J. G. Webster, Medical Instrumentation Application and Design, 3rd ed., John Wiley and Sons, Inc., USA, 1998.
- 2. C. Kitchin, L. Counts, A Designer's Guide to Instrumentation Amplifiers, 3rd ed. Analog Devices, Inc., 2006.
- 3. C. Toumazou, F. J. Lidgey, and C.A. Makris. "Current-mode instrumentation amplifier," Short Run Press Ltd., Exeter, 1993.
- 4. K. Koli and K. Halonen, "CMRR enhancement techniques for current-mode instrumentation amplifiers," IEEE Transactions on Circuits and Systems-I: Fundamental Theory and Applications, vol. 47, no. 5, May 2000
- 5. M. Lorenzo and A. Manzano, "Design and implementation of CMOS rail-to-rail operational amplifiers," Department of Electrical and Electronics Engineering, University of the Philippines, October 2006.
- 6. P.R. Gray, P.J. Hurst, S.H. Lewis, and R.G. Meyer, Analysis and Design of Analog Integrated Circuits, 4th ed., John Wiley and Sons, Inc., USA, 2001.
- 7. A. Sedra and G. Roberts, "Current conveyor theory and practice," Analogue IC Design: The Current-mode Approach, Short Run Press Ltd., Exeter, 1993.
- 8. S. J. Azhari and H. Fazlalipoor, "A novel current mode instrumentation amplifier (CMIA) topology," IEEE Transactions on Instrumentation and Measurement, vol. 49, no. 6, December 2000.
- 9. A. A. Khan, M. A. Al-Turiagi and M. A. El-Ela, "An improved current-mode instrumentation amplifier with bandwidth independent of Gain," IEEE Transactions on Instrumentation and Measurement, vol. 44, no. 4, August 1995.
- 10. INA326 Datasheet, http://www.ti.com/lit/ds/sbos222d/sbos222d.pdf.